Journal of
Materials in Life Sciences

Vol. 5 No. 1 (2026)

Full Paper

Effect of Linkers in Palladium Reduced Graphene Oxide as Catalyst in Hydrogenation Under Electric Field: Experimental and Computational Study

Siti Aisyah Zulaikha Binti Zulkefli[a], Fazira Ilyana Abdul Razak[a,b], Juan bin Matmin[a], Roichatul Madinah[a], Yee Shi Wee[a]

[a]Department of Chemistry, Faculty of Science, Universiti Teknologi Malaysia, 81310 UTM Johor Bahru, Johor, Malaysia.
[b]Department of Physics, Faculty of Science and Technology, Universitas Airlangga, 60115 Surabaya, Indonesia

Article history
Received
10 March 2026
Revised
12 April 2026
Accepted
1 May 2026
Published online
30 May 2026

*Corresponding author
fazirailyana@utm.my

Abstract

Hydrogenation is an important industrial process that commonly requires high temperatures and pressures, leading to high energy consumption and catalyst deactivation. In this study, the effects of different linker systems on palladium–reduced graphene oxide (Pd/rGO) catalysts for hydrogenation under an external electric field (EEF) were investigated. Polyvinylpyrrolidone (PVP), polypyrrole (PPy), and chitosan (CS) were used as linkers in the synthesis of Pd–rGO catalysts. The prepared catalysts were characterized using ATR-FTIR, SEM, and ICP-OES analyses to evaluate chemical interactions, morphology, and palladium loading. ICP-OES results showed that Pd–CS/rGO exhibited the highest Pd loading of 4.58 wt%, indicating stronger Pd immobilization by the amino and hydroxyl functional groups of chitosan. Catalytic performance was evaluated through the hydrogenation of 1-octene under EEF-assisted conditions and analyzed using GC-FID. Among the investigated catalysts, Pd–CS/rGO showed the highest catalytic activity with 11.3% conversion. Density-functional theory calculations further revealed differences in the electronic distribution and electrostatic characteristics of the linkers, which were generally consistent with the experimental observations. Overall, linker chemistry was found to influence Pd incorporation, electronic behavior, and catalytic performance under external electric field conditions.

Keywords : Density-functional theory, External electrical field, Hydrogenation, Linker, Palladium, Reduce graphene oxide

© 2026 Penerbit UTM Press. All rights reserved

1.0 INTRODUCTION

Hydrogenation is an important chemical process widely used in the synthesis of fine chemicals [1-2], pharmaceuticals [2-5], and energy storage materials [6-8]. Conventional hydrogenation processes often require harsh operating conditions involving high temperatures and pressures. These severe conditions result in high energy consumption, increased carbon emissions, and rapid catalyst deactivation. Therefore, the efficiency of hydrogenation reactions strongly depends on the development of effective catalysts capable of promoting hydrogen addition under mild conditions. Palladium (Pd) is widely used as a hydrogenation catalyst because of its exceptional ability to activate hydrogen molecules and facilitate hydrogen in addition to unsaturated bonds such as alkenes and alkyne [9-11]. Compared with other transition metals, Pd exhibits superior catalytic activity, selectivity, and versatility under relatively mild reaction conditions. To further improve its catalytic performance, stability, and recyclability, Pd is commonly supported on nanostructured materials [12].

To further improve the catalytic performance and stability of hydrogenation catalysts, reduced graphene oxide (rGO) has attracted considerable attention as a promising support material for Pd due to its unique structural and electronic properties. rGO provides a large surface area, high electrical conductivity, and abundant defect sites, which facilitate the stabilization and uniform dispersion of metal particles [13]. In addition, the oxygen-containing functional groups and defect-rich structure of rGO promote strong metal–support interactions, which can reduce Pd particle aggregation and metal leaching during catalytic reactions [14]. The excellent electron mobility of rGO also enhances charge transfer between Pd and the support, thereby improving catalytic activity and reaction efficiency [15]. As a result, Pd–rGO hybrid catalysts exhibit enhanced hydrogenation performance owing to improved accessibility of active sites and more efficient electron transfer during the catalytic process [16].

Recently, the application of EEFs has gained increasing attention as an alternative approach for improving catalytic efficiency and reducing the dependence on harsh reaction conditions. EEFs can alter the energy landscape of reaction intermediates, induce polarization of chemical bonds, and influence charge carrier distribution within catalytic systems. Previous studies have shown that EEFs can affect hydrogen adsorption behavior and modify the electronic properties of catalyst surfaces, particularly in Pd-based catalytic systems [17-20]. In Pd-based catalysts, EEFs have been reported to modify the adsorption energies of reactants and hydrogen species, thereby promoting or suppressing specific reaction pathways. In Pd/rGO systems, the presence of an electric field may enhance hydrogen adsorption and facilitate hydrogen dissociation on the catalyst surface, leading to improved catalytic activity and hydrogenation performance. This field-assisted approach enables dynamic modulation of catalytic activity without altering the chemical composition of the catalyst system [21].

The performance of immobilized Pd–rGO systems is strongly influenced by the type of linker used to bind the catalyst to the substrate. Linkers play important roles in determining the mechanical stability, chemical compatibility, and electronic communication between the catalyst and the support. Polymeric linkers such as polyvinylpyrrolidone (PVP), polypyrrole (PPy), and chitosan are widely used because of their ability to stabilize particles and facilitate catalyst immobilization through covalent or non-covalent interactions. PVP is commonly used as a stabilizing agent to achieve uniform Pd dispersion, whereas PPy, as a conductive polymer, can enhance electron transfer between Pd and rGO. Chitosan, a naturally derived polymer containing amino and hydroxyl functional groups, provides strong metal anchoring and excellent film-forming properties [22]. Depending on the surface functionality of the substrate, linker attachment may occur through covalent bonding, such as amide or ester linkages, or through non-covalent interactions including electrostatic attraction and π–π stacking. Despite their importance, systematic studies evaluating the influence of different linker systems on catalyst stability, catalytic activity, and electron transport under operating conditions remain limited [16].

By integrating experimental and computational approaches, this study aims to evaluate the catalytic behavior of linker-modified Pd–rGO catalysts supported on cotton textile under external electric fields. Cotton textile has been reported as a promising support material for Pd/rGO catalysts due to its hierarchical porosity, natural hydroxyl functionality, and flexibility, which facilitate uniform electric field distribution and improved mass diffusion during hydrogenation reactions [23]. However, studies investigating the combined effects of external electric fields, linker chemistry, and textile-supported Pd–rGO catalysts on hydrogenation performance remain limited.

2.0 EXPERIMENTAL

This experimental procedure consists of four parts which is the synthesis of Pd-rGO, synthesis of Pd-rGO with linker, hydrogenation of octene with presence of external electric field and computational study on Pd-rGO and linker system.

2.1 Materials

Graphene oxide (GO), palladium chloride ($PdCl_2$, ≥99.9%), sodium borohydride ($NaBH_4$), ethanol (CH_3CH_2OH, ≥99.8%), phosphoric acid (H_3PO_4), pyrrole monomer (C_4H_5N), ammonium persulfate [$(NH_4)_2S_2O_8$], methanol (CH_3OH), hydrazine hydrate ($N_2H_4{\cdot}H_2O$), sodium hydroxide (1 M NaOH), chitosan ($(C_6H_{11}NO_4)_n$), acetic acid solution (3%, CH_3COOH), and hydrazine ($N_2H_4{\cdot}H_2O$) were purchased from Sigma-Aldrich. Polyvinylpyrrolidone (PVP, $(C_6H_9NO)_n$) was obtained from QReC, while ethylene glycol [$(CH_2OH)_2$] was supplied by Honeywell Riedel-de Haën. Deionized water (H_2O) was used throughout the study.

2.2 Synthesis of Pd-rGO: without and with linkers

Pd-rGO

Graphene oxide (GO, 0.03 g) was dispersed in distilled water (150 mL) by ultrasonication for 30 minutes. Subsequently, $PdCl_2$ solution (6.0 mL, 0.885 mg mL^{-1}) was added to the GO suspension, followed by ultrasonication for 2 hours to promote the interaction between Pd ions and GO sheets [24]. Freshly prepared $NaBH_4$ solution (6.0 mL, 0.2 M) was then added dropwise, and the reaction mixture was continuously stirred at room temperature for 24 hours. The resulting Pd–rGO product was collected by centrifugation and washed several times with distilled water and ethanol to remove residual $PdCl_2$ and unsupported Pd particles [24]. Finally, the product was dried in an oven at 50°C overnight.

First linker: polyvinylpyrrolidone* (*Pd-PVP/rGO)
GO (0.06 g) was dispersed in deionized water (50 mL) containing polyvinylpyrrolidone (PVP, 0.0071 g) and sonicated at room temperature for 1 hour [25]. Subsequently, $PdCl_2$ solution (10 wt.% in 10 wt.% HNO_3, 99.999%, 1000 µL) was added to the suspension, and the mixture was stirred for 3 hours. Ethylene glycol (154.9 mL) was then slowly introduced as both a stabilizing and reducing agent. The resulting mixture was heated under microwave irradiation (1000 W) for 12 minutes. The obtained dark black product was filtered and washed several times with hot deionized water (40 mL) and ethanol (10 mL) to remove residual impurities. Finally, the product was dried in an oven at 80°C overnight [25].

Second linker: polypyrrole (Pd-PPy/rGO)
GO (0.12 g) and cetyltrimethylammonium bromide (CTAB, 0.273 g) were dispersed in deionized water (100 mL) and sonicated for 30 minutes [26]. A mixture of phosphoric acid and pyrrole monomer (45 mL, 0.0047 mol L^{-1}) was added gradually, and the solution was stirred for 2 hours at 15°C. Polymerization was initiated by the slow addition of ammonium persulfate (APS, 0.141 g), followed by continuous stirring for 4 hours at the same temperature. The resulting black precipitate was filtered, washed with methanol, and dried under vacuum. To prepare rGO/PPy, the dried GO/PPy sample was reduced using hydrazine hydrate. For Pd loading, rGO/PPy powder (0.25 g) was dispersed in ethylene glycol (30 mL) by ultrasonication for 1 hour. $PdCl_2$ solution (7 mg mL^{-1}) was then added under vigorous stirring, and the pH of the mixture was adjusted to 7 using 1 M NaOH solution. The suspension was subsequently subjected to microwave irradiation using a conventional microwave oven (1000 W, 2.45 GHz) at 30 s intervals for a total of 2 minutes. The resulting slurry was centrifuged, washed with deionized water, and dried under vacuum at 100°C [26].

Third linker: chitosan (Pd-CS/rGO)
Chitosan (CS, 0.4 g, >400 mPa·s) was dissolved in 3% acetic acid solution (40 mL) under continuous stirring, followed by the addition of GO solution (100 mL, 4.0 mg mL^{-1}) [27]. After stirring for 2 hours, the mixture was heated to 85°C, and hydrazine hydrate (10 mL, $N_2H_4 \cdot H_2O$) was added as a reducing agent. The reaction mixture was stirred for 24 hours, during which the solution color gradually changed from brown to black, indicating the reduction of GO. The pH of the suspension was then adjusted to approximately 9 using 1.0 M NaOH solution. The resulting precipitate was collected by centrifugation (6000 rpm), washed repeatedly with deionized water until neutral pH was achieved, and freeze-dried to obtain CS–rGO. For the preparation of Pd–CS/rGO, $PdCl_2$ (0.0531 g) was first dissolved in HCl solution (51.30 mL, 2.0 mol L^{-1}) and diluted with deionized water (40 mL). The pH of the solution was adjusted to 6 by dropwise addition of 1.0 M NaOH under mechanical stirring. Subsequently, CS–rGO (0.5 g) was added to the Pd-containing solution and stirred until the supernatant became colorless. Freshly prepared $NaBH_4$ solution (0.0141 g in 25.60 mL deionized water) was then added under continuous stirring, and the mixture was further stirred for 12 hours. Finally, the obtained solid product was washed with deionized water and dried at 45°C [27].

2.3 Characterization

Attenuated Total Reflectance Fourier Transform Infrared (ATR-FTIR)
ATR-FTIR spectroscopy was used to qualitatively identify the functional groups present in Pd/rGO, Pd–PVP/rGO, Pd–PPy/rGO, and Pd–CS/rGO composites. The spectra were recorded using a PerkinElmer FTIR spectrometer (Series 1600). Approximately 1–2 mg of dry catalyst powder was directly placed onto the ATR crystal without additional sample preparation. For each sample, 32 scans were collected in the wavenumber range of 4000–400 cm^{-1} with a spectral resolution of 4 cm^{-1} to improve the signal-to-noise ratio. Background spectra were recorded prior to each measurement.

Inductively Coupled Plasma Optical Emission Spectroscopy (ICP-OES)
ICP-OES was employed to determine the palladium loading and evaluate the metal incorporation efficiency in the Pd/rGO catalysts. Approximately 10–20 mg of catalyst sample was digested using a mixture of concentrated nitric acid (HNO_3) and hydrochloric acid (HCl) under controlled heating conditions until complete dissolution was achieved. The resulting solution was diluted to a known final volume using deionized water. Standard palladium solutions with known concentrations were used to establish calibration curves. The emission intensity of Pd at its characteristic wavelength was measured under optimized plasma conditions, and the Pd content was calculated and expressed as weight percentage relative to the total catalyst mass.

Scanning Electron Microscopy (SEM)
Scanning Electron Microscopy (SEM) analysis was carried out to examine the surface morphology, structural features, and Pd dispersion of the Pd/rGO catalysts using a JEOL JSM-5510LV microscope. A small amount of catalyst powder was dispersed onto conductive carbon tape mounted on an aluminum stub. Prior to imaging, the samples were sputter-coated with a thin conductive layer to minimize charging effects during analysis. SEM images were obtained under high-vacuum conditions at various magnifications, which were x500, x1500, and x5000, using an accelerating voltage ranging from 5 to 20 kV. The morphology of the rGO sheets, surface texture, and degree of particle aggregation were qualitatively evaluated. In addition, the dispersion of Pd on the rGO surface and the morphological differences among catalysts containing different linker systems were compared.

2.4 Hydrogenation of octene under the influence of external electric field (EEF)

The hydrogenation setup is illustrated in Figure 1. Prior to catalyst coating, the cotton fabric was subjected to a scouring treatment using anhydrous sodium carbonate (Na_2CO_3). The treated fabric was then immersed in the Pd–rGO dispersion and sonicated for 30 min, followed by drying at 55 °C for 1 h. This coating process was repeated 10 times to achieve uniform catalyst deposition on the textile surface. The EEF-assisted hydrogenation system was assembled using H-TEC Education's 1-Cell Rebuildable Polymer Electrolyte Membrane Electrolyzer Kit and a PeakTech P6120 AC/DC laboratory power supply. The catalyst-coated textile was positioned inside the electrolyzer and used as the catalytic platform. The system was connected to a DC power supply and supplied with H_2 gas at a constant flow rate of 30 mL min^{-1}. Subsequently, 3 mL of 1-octene was introduced into the system, and the hydrogenation reaction was carried out for 3 min. After the reaction, the hydrogenated product was collected in a vial, and the catalyst-coated textile was rinsed with hexane to recover any remaining product. The same procedure was repeated for Pd–PVP/rGO, Pd–PPy/rGO, and Pd–CS/rGO catalysts. In Figure 1, the cotton textile coated with reduced graphene oxide was replaced with cotton textile coated with Pd–rGO catalysts.

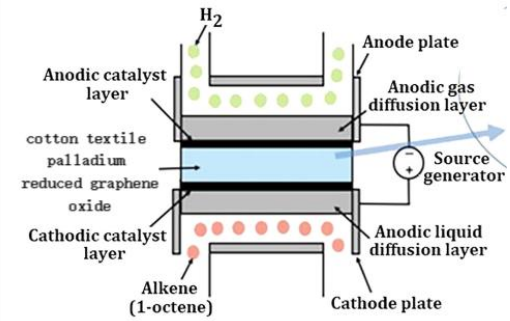


Figure 1 : Illustration of the 1-octane hydrogenation set up with the presence of external electric field (EEF)

2.5 Density-functional calculations

All calculations were performed using DFT implemented in the Gaussian16 program package [28]. To simplify the computational model while retaining the key electronic characteristics of the linker systems, the monomer forms of the three linkers were used to represent the corresponding polymeric linkers. The selected monomer structures preserve the main functional groups responsible for interaction with Pd species and charge distribution behavior. Geometry optimization was carried out using the B3LYP functional with the LanL2DZ basis set. This exchange-correlation functional has been widely used for the studies of graphene-based material [23, 29, 30]. The optimized structures were subsequently used for electronic structure analysis, including Molecular Electrostatic Potential (MEP) mapping and Highest Occupied Molecular Orbital (HOMO)–Lowest Unoccupied Molecular Orbital (LUMO) analysis, to evaluate the electronic characteristics and charge distribution of the linker systems relevant to Pd–rGO catalysis.

3.0 RESULTS AND DISCUSSION

3.1 ATR-FTIR Analysis

Figure 2 presents the ATR-FTIR spectra of Pd/rGO catalysts synthesized using three different linker systems: PVP, PPy, and chitosan. The spectra were evaluated to confirm the successful incorporation of the linker molecules and to understand the bonding interactions between the Pd, rGO, and the polymer matrices. For all samples, the broad absorption bands observed in the 3200–3500 cm^{-1} range are assigned to O−H and N−H stretching vibrations. The more pronounced O–H and N–H stretching bands observed for Pd/PPy/GO can be attributed to the presence of pyrrolic nitrogen atoms in the PPy chains and their interaction with residual oxygen-containing groups on the GO surface. These functional groups promote intermolecular hydrogen bonding, resulting in band broadening and increased absorption intensity in the 3200–3500 cm^{-1} region. Furthermore, the polymeric nature of PPy provides a larger number of surface-active sites capable of retaining adsorbed water molecules, which may further contribute to the enhanced O–H stretching absorption.

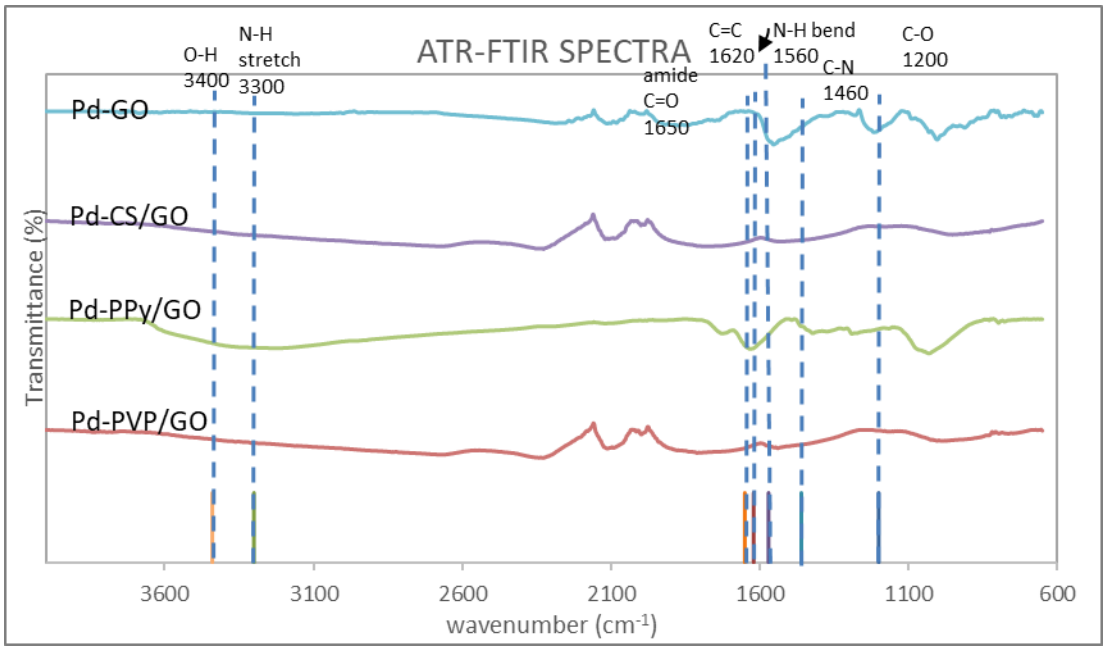


Figure 2 : Attenuated Total Reflectance Fourier Transform Infrared (ATR-FTIR) spectra for Pd/GO the blue line, Pd-PVP/rGO (polyvinylpyrrolidone) the red line, Pd-PPy/rGO (polypyrrole) the green line, and Pd-CS/rGO (chitosan) the purple line

In Pd-PVP/rGO, a distinctive peak corresponding to the C=O stretching vibration of the pyrrolidone ring appears around 1650 cm^{-1}. The appearance of this peak, along with its minor shift compared to pure PVP, indicates a coordination interaction between the carbonyl groups of PVP and the surface of the Pd. Meanwhile, Pd-PPy/rGO displays characteristic C–N stretching and ring vibrations within the 1300–1550 cm^{-1} region. These distinct features verify that the polypyrrole matrix was successfully integrated onto the rGO support. The preservation of these sharp PPy bands shows that the conductive polymer backbone remains stable and intact after metal deposition.

For Pd-CS/rGO, distinct absorption bands emerge for N–H bending around 1550–1600 cm^{-1} and C–O stretching near 1020–1080 cm^{-1}. These specific peaks confirm the integration of chitosan functional groups, particularly the amine and hydroxyl networks known for chelating transition metals. Notably, the bands in the chitosan spectrum appear broader and more intense compared to the PVP and PPy systems. This structural difference indicates a higher degree of localized interaction between the Pd and the chitosan matrix. This enhanced chemical binding is expected to improve palladium stabilization and minimize potential metal leaching during catalytic testing.

3.2 ICP-OES results

ICP-OES was used to quantify the Pd content of the synthesized Pd-rGO with the presence of linkers and to evaluate the efficacy of linker systems in immobilizing Pd. The analysis utilized a calibration curve (0.05–1.00 mg L^{-1}) with excellent linearity (R^2 = 0.99998), and quality control samples showed recoveries of approximately 100%, confirming measurement reliability. As shown in Table 1, the Pd loading varied significantly depending on the linker system: Pd-PVP/rGO contained 0.31 w% Pd, whereas Pd-CS/rGO contained 4.58 w%.

Table 1 : Weight percentage of Pd (w%) in different linkers: polyvinylpyrrolidone (Pd-PVP/rGO) and chitosan (Pd-Cs/rGO)

No.	Catalyst	Weight Percentage of Pd (w%)
1.	Pd-PVP/rGO	0.31
2.	Pd-CS/rGO	4.58

Pd–PVP/rGO catalyst showed a Pd loading of 0.31 w%, with a low relative standard deviation (RSD = 1.00%) and acceptable repeatability. This relatively low Pd content indicates that although PVP is effective in regulating the dispersion of Pd nanoparticles, its interaction with Pd is primarily weak and non-covalent. Consequently, less Pd is anchored on the rGO surface, resulting in reduced metal loading. In contrast, the chitosan-linked Pd–rGO catalyst exhibited a substantially higher Pd loading of 4.58 w% with a low RSD of 0.60%. This significant increase in Pd concentration highlights chitosan's strong chelation

capacity, as its abundant amine and hydroxyl functional groups can coordinate Pd ions during synthesis. The strong chemical interaction between chitosan and Pd enhances metal immobilization and minimizes Pd loss during sample preparation and washing.

Although ICP-OES data for Pd–PPy/rGO are not shown, qualitative comparison based on synthesis behavior and scanning electron microscopy (SEM) morphology suggests an intermediate Pd loading, where PPy provides sufficient anchoring while maintaining electrical conductivity. Overall, the ICP-OES results demonstrate that linker chemistry plays a crucial role in determining Pd loading and metal utilization efficiency.

3.3 SEM analysis

Figure 3 shows the surface morphology and dispersion of Pd–rGO catalysts prepared with different linker systems, examined by scanning electron microscopy (SEM) at magnifications of x500, x1500, and x5000. At low magnification (×500), the Pd-PVP/rGO sample exhibited relatively smooth, layered rGO sheets with minimal aggregation, indicating good exfoliation and a uniform coating. In contrast, Pd-PPy/rGO showed a rougher, more granular surface, attributed to the PPy coating forming a continuous conductive network over the rGO sheets. Pd-CS/rGO displayed a compact, textured morphology, consistent with a chitosan-based matrix embedding rGO and Pd nanoparticles. Meanwhile, at intermediate magnification (x1500), Pd-PVP/rGO presented finely dispersed features without large Pd agglomerates, as evidenced by small white dots, confirming the stabilizing role of PVP. Pd–PPy/rGO exhibited interconnected nodular structures, suggesting uniform PPy growth and effective Pd anchoring within the polymer network. Pd–CS/rGO showed denser domains, correlating with higher Pd loading but also indicating partial encapsulation of Pd by chitosan.

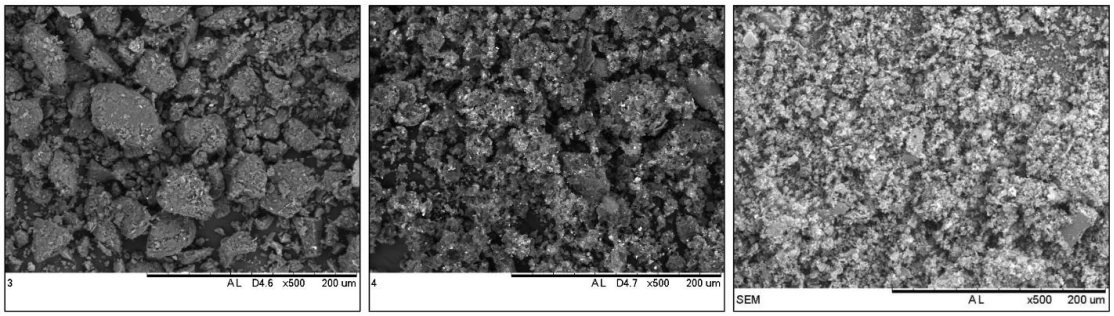
At high magnification (x5000), Pd-PVP/rGO maintained relatively uniform dispersion, although individual Pd nanoparticles were difficult to resolve owing to their small size. Pd-PPy/rGO displayed well-distributed features, supporting strong Pd-PPy/rGO interactions and good electrical connectivity. Pd-CS/rGO revealed clustered regions, which may reduce Pd accessibility but enhance mechanical stability and resistance to leaching. Specifically, the PVP-linked catalyst exhibited a smooth, continuous surface with finely dispersed Pd particles, confirming that PVP acts as an effective stabilizer by regulating particle growth. However, areas of lower particle density were also observed, suggesting weak anchoring between Pd and the rGO support. This primary physical interaction may account for the lower metal loading and increased susceptibility to Pd leaching during catalysis.

The PPy-linked catalyst showed a more interconnected and textured morphology, with rGO sheets partially coated by a polymeric PPy network that incorporated Pd particles, thereby enhancing surface coverage and electrical connectivity. The conjugated PPy backbone facilitates electronic communication between Pd and rGO, a feature particularly beneficial for electric-field-assisted hydrogenation, where efficient charge redistribution is required. The chitosan-linked catalyst exhibited a denser, rougher morphology. Aggregated but well-anchored Pd domains were observed, indicating strong interactions between Pd and the amine/hydroxyl functional groups of chitosan. The increased surface coverage reflects enhanced Pd immobilization, consistent with chitosan's chelating capacity. Although some particle clustering was visible, this morphology is expected to improve catalyst stability and reduce metal leaching, despite a slight decrease in active site accessibility.

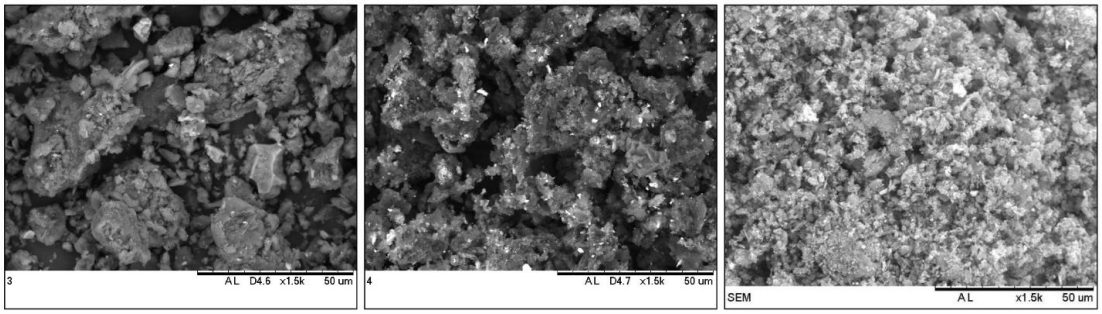
Overall, the SEM results demonstrate that linker chemistry profoundly influences catalyst morphology. PVP promotes fine dispersion but weak anchoring, PPy generates interconnected and conductive structures, and chitosan enhances Pd immobilization through strong chemical interactions. These morphological differences provide a structural basis for the variations in Pd loading, stability, and catalytic efficiency observed in ICP-OES and hydrogenation studies.

3.4 Catalytic hydrogenation under EEF

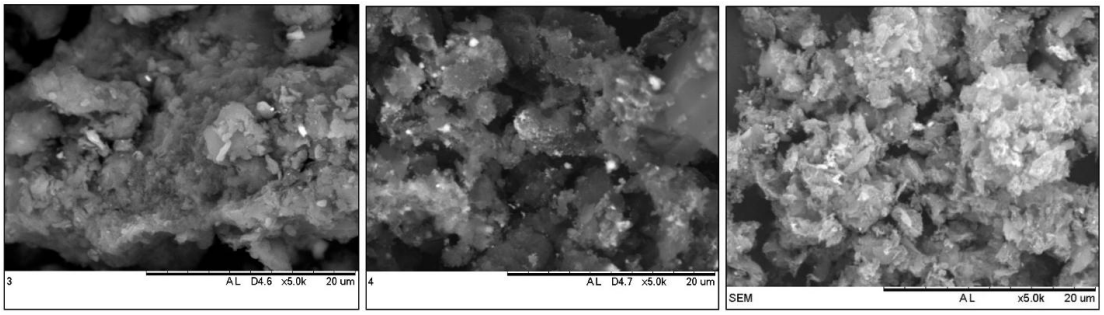
The catalytic performance of the Pd/rGO catalysts was evaluated through the hydrogenation of 1-octene, and the results are summarized in Table 2. Among the catalysts studied, Pd–CS/rGO exhibited the highest catalytic activity, achieving 11.3% conversion of 1-octene to octane. The enhanced activity of Pd–CS/rGO is likely associated with its higher Pd loading, as determined by ICP-OES analysis (see Table 1), where Pd–CS/rGO showed significantly greater Pd incorporation compared with the other linker systems. The amino and hydroxyl functional groups of chitosan may provide stronger coordination with Pd species during catalyst synthesis, resulting in improved Pd immobilization and a higher density of accessible active sites.



(a) x500 magnification



(b) at x1,500 magnification



(c) at x5,000 magnification

Figure 3 : Scanning electron microscopy (SEM) image for Pd-PVP/rGO (polyvinylpyrrolidone; left), Pd-PPy/rGO (polypyrrole; middle), and Pd-CS/rGO (chitosan; right) at (a) x500, (b) x1,500, and (c) x5,000 magnification

Table 2 : GC-FID analysis of 1-octene hydrogenation over Pd/rGO with different linker systems: polyvinylpyrrolidone (PVP), polypyrrole(PPy), and chitosan (CS) under an external electric field

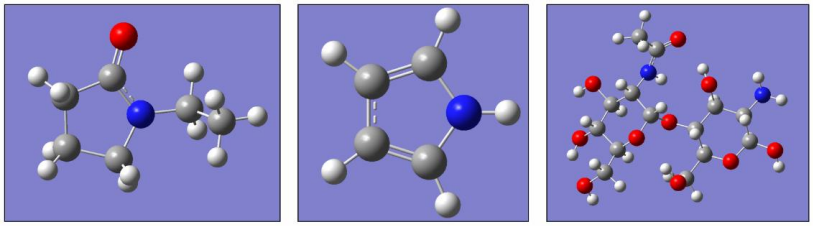
No.	Catalyst	Concentration of n-octene (mg/mL)	Concentration of n-octane (mg/mL)	Conversion of octene to octane (%)
1.	Pd-PVP/rGO	400.1563	0.3105	0.08
2.	Pd-PPy/rGO	333.2710	1.0680	0.32
3.	Pd-CS/rGO	1.8847	0.2413	11.3

Pd–PPy/rGO exhibited moderate catalytic performance, which is 0.32%, compared with the other catalysts. The conductive nature of the PPy linker may facilitate electron transfer and enhance H_2 activation under the applied external electric field. In addition, the nodular surface morphology observed from SEM analysis suggests relatively good dispersion and interaction between Pd and the PPy-modified rGO support. However, the lower catalytic activity compared with Pd–CS/rGO indicates that Pd incorporation and active site availability may still be limited in the PPy-based system. Meanwhile, Pd–PVP/rGO showed the lowest catalytic activity, with only 0.08% conversion of 1-octene. The low performance may be attributed to insufficient Pd loading and weaker interactions between Pd and the rGO support. Although PVP can act as a stabilizing agent

during synthesis, excessive surface coverage or limited Pd anchoring may reduce the accessibility of catalytic active sites. The high residual concentration of n-octene after reaction further suggests limited hydrogenation efficiency under the applied reaction conditions.

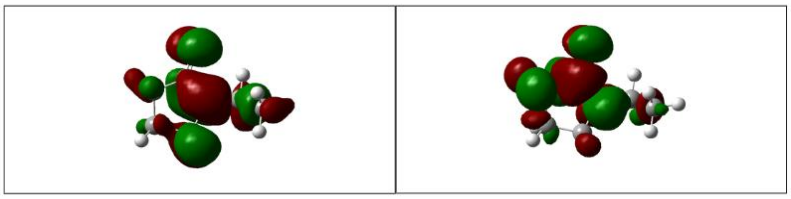
3.5 HOMO–LUMO Analysis of three different linker monomers

Figure 4 shows the optimized structures of the linker monomers obtained from the DFT calculations. The corresponding HOMO–LUMO plots in reveal distinct electronic characteristics for each linker monomer, which may influence their interactions with Pd and the rGO support as shown in Figure 5. For the vinylpyrrolidone, as shown in Figure 5a, the HOMO is mainly localized around the carbonyl-containing pyrrolidone ring, whereas the LUMO is distributed along the vinyl group. This orbital distribution suggests that vinylpyrrolidone mainly interacts with Pd through coordination at the carbonyl oxygen, with limited electron delocalization across the molecule. Such electronic behavior may contribute to the relatively weak enhancement of catalytic performance observed under the external electric field despite the good dispersion of Pd.

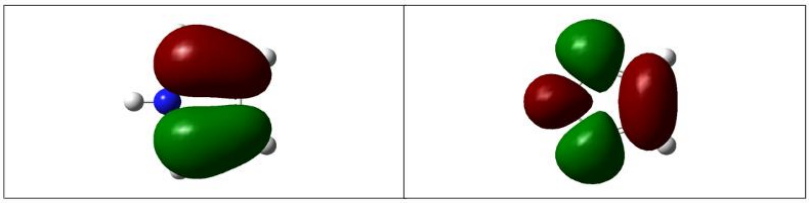


(a) Vinylpyrrolidone (a) Pyrrole (b) Chitosan

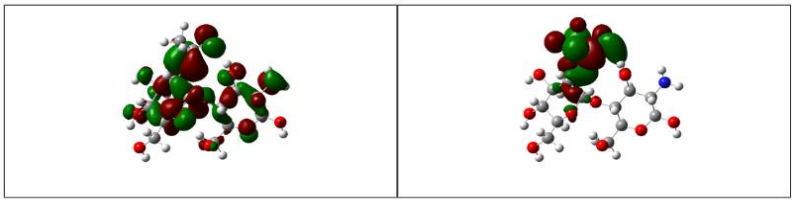
Figure 4 : The optimized structure of monomer forms from three different linkers



(a) Vinylpyrrolidone monomer



(b) pyrrole monomer



(c) Chitosan monomer

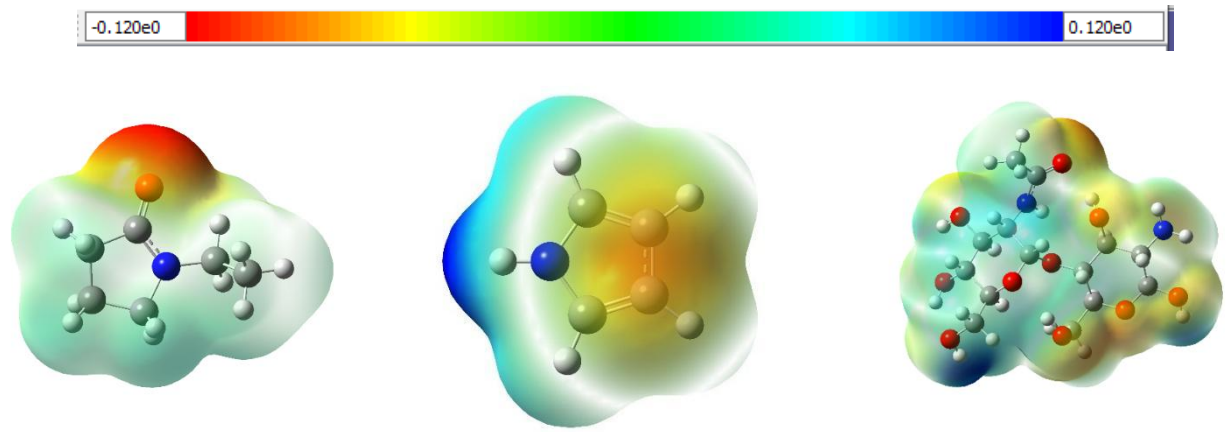
Figure 5. The HOMO (left) – LUMO (right) mapping of the monomer form from three different linkers

In contrast, the pyrrole shows HOMO and LUMO distributions spread across the conjugated pyrrole ring as shown in Figure 5b. The overlap between these orbitals suggests relatively good electronic mobility and charge transfer capability within the molecule. These properties may support electron redistribution between Pd and the rGO support under the applied electric field, which could contribute to the improved catalytic performance observed for the Pd–PPy/rGO system during hydrogenation. For the chitosan, which can be seen from Figure 5c, the HOMO is primarily localized around the amino and hydroxyl functional groups, whereas the LUMO is mainly distributed along the saccharide backbone. The presence of electron-rich functional groups

indicates a strong tendency for interaction with Pd species, which may assist Pd immobilization and catalyst stability. However, the non-conjugated structure of chitosan may limit electron delocalization compared with the pyrrole system.

3.6 Molecular electrostatic potential (MEP) maps

The Molecular Electrostatic Potential (MEP) maps in Figure 6 provide additional insight into the charge distribution of the linker monomers and their potential interactions with Pd species. For the vinylpyrrolidone, a relatively negative electrostatic potential is observed around the carbonyl oxygen atom, suggesting the presence of localized coordination sites for Pd binding. However, the overall charge distribution appears relatively uniform, which may indicate limited contribution to long-range charge transfer within the system.



(a) Vinylpyrrolidone monomer (b) Pyrrole monomer (c) Chitosan monomer

Figure 6 : The Molecular Electrostatic Potential (MEP) maps of the monomer form from three different linkers: (a) vinylpyrrolidone, (b) pyrrole, and (c) chitosan

In contrast, pyrrole exhibits broader regions of negative electrostatic potential distributed across the conjugated pyrrole ring. This distribution suggests a greater ability to support charge delocalization and electron mobility throughout the molecule. Such characteristics may contribute to improved electron transfer and enhanced responsiveness of the catalyst system under the applied external electric field. For chitosan, the negative electrostatic potential is mainly localized around the amino and hydroxyl functional groups. This localized charge distribution indicates strong interaction capability with Pd species and may support improved Pd immobilization within the catalyst system. However, compared with pyrrole, the more localized nature of the charge distribution may limit electron mobility under external electric field conditions.

4.0 CONCLUSION

In this study, the effects of different linker systems on the performance of palladium–reduced graphene oxide (Pd–rGO) catalysts under an external electric field (EEF) were successfully investigated. Pd–rGO catalysts incorporating polyvinylpyrrolidone (PVP), polypyrrole (PPy), and chitosan (CS) linkers were synthesized and characterized using ATR-FTIR, SEM, and ICP-OES analyses. The characterization results confirmed successful incorporation of the linker systems and showed that linker chemistry influenced catalyst morphology and Pd incorporation. ICP-OES analysis revealed that Pd–CS/rGO exhibited the highest Pd loading (4.58 wt%), indicating stronger interaction between Pd species and the amino and hydroxyl functional groups of chitosan during catalyst synthesis. Catalytic evaluation through the hydrogenation of 1-octene under EEF-assisted conditions also showed that Pd–CS/rGO achieved the highest conversion (11.3%), while Pd–PPy/rGO and Pd–PVP/rGO exhibited lower conversions of 0.32% and 0.08%, respectively.

DFT calculations revealed differences in the electronic distribution and electrostatic characteristics of the linker monomers. The HOMO–LUMO and MEP analyses showed that pyrrole exhibited more delocalized electronic distribution across the conjugated pyrrole ring, whereas the chitosan monomer showed more localized electron density around the amino and hydroxyl functional groups. In contrast, vinylpyrrolidone displayed relatively localized electronic distribution mainly around the carbonyl-containing pyrrolidone ring. These differences in electronic characteristics may influence the interaction between the linker systems and Pd; and were generally consistent with the experimental observations on Pd incorporation and catalytic performance.

Acknowledgment

This project was funded by the Ministry of Higher Education, Malaysia, for the Fundamental Research Grant Scheme FRGS (PY/2025/02278/R.J130000.7854.5F764). Author thanks the Centre for Information and Communication Technology (CICT),

Universiti Teknologi Malaysia for supporting and providing high-performance computing facilities and services that expedited the research.

References

[1] Blaser, H.-U., Malan, C., Pugin, B., Spindler, F., Steiner, H., & Studer, M. (2002). Selective hydrogenation for fine chemicals: Recent trends and new developments. Advanced Synthesis & Catalysis, 345(1–2), 103–151.

[2] Machado, R. M., Heier, K. R., & Broekhuis, R. R. (2001). Developments in hydrogenation technology for fine-chemical and pharmaceutical applications. Current Opinion in Drug Discovery & Development, 4(6), 745–755.

[3] Wojcik, B., & Adkins, H. (1934). Catalytic hydrogenation of amides to amines. Journal of the American Chemical Society, 56(11), 2419–2424. https://doi.org/10.1021/ja01326a061

[4] Saudan, L. A. (2007). Hydrogenation processes in the synthesis of perfumery ingredients. Accounts of Chemical Research, 40(12), 1309–1319. https://doi.org/10.1021/ar700140m

[5] Steven, A. (2024). Heterogeneous hydrogenation in pharmaceutical development. In T. I. Shabatina & Y. Gromova (Eds.), Adsorption: Fundamental mechanisms and applications (Ch. 7). IntechOpen. https://doi.org/10.5772/intechopen.1007431

[6] Chibani, A., Boucetta, C., Merouani, S., Tounsi, A., Adjela, S., Lamiri, L., Bouchoula, B., & Merabtia, H. (2024). Impact of fins and cooling fluid on the hydrogenation process in a $LaNi_5$-based metal hydride reactor for hydrogen storage. International Journal of Hydrogen Energy, 69, 134–146. https://doi.org/10.1016/j.ijhydene.2024.04.314

[7] Gordeeva, N. A., Shesterkina, A. A., Vikanova, K. V., & Kustov, A. L. (2024). Naphthalene and its derivatives hydrogenation for hydrogen storage: Comparative analysis of the role of noble and non-noble metal catalysts – A review. International Journal of Hydrogen Energy, 69, 147–165. https://doi.org/10.1016/j.ijhydene.2024.04.340

[8] Zamljen, A., Lavrič, Ž., Prašnikar, A., Teržan, J., Grilc, M., Meden, A., & Likozar, B. (2024). Understanding platinum-based H_2 adsorption/desorption kinetics during catalytic hydrogenation or hydrogen storage-related reactions. Renewable Energy, 226, 120467. https://doi.org/10.1016/j.renene.2024.120467

[9] Borodziński, A., & Bond, G. C. (2008). Selective hydrogenation of ethyne in ethene-rich streams on palladium catalysts, Part 2: Steady-state kinetics and effects of palladium particle size, carbon monoxide, and promoters. Catalysis Reviews, 50(3), 379–469. https://doi.org/10.1080/01614940802142102

[10] Borodziński, A., & Bond, G. C. (2006). Selective hydrogenation of ethyne in ethene-rich streams on palladium catalysts. Part 1. Effect of changes to the catalyst during reaction. Catalysis Reviews, 48(2), 91–144. https://doi.org/10.1080/01614940500364909 [11] Lan, X., Chen, J. G., & Wang, T. (2025). Recent advances in thermocatalytic acetylene selective hydrogenation. Chemical Society Reviews, 54(15), 1234–1256. https://doi.org/10.1039/d4cs01237b

[12] Zhao, X., Chang, Y., Chen, W.-J., Wu, Q., Pan, X., Chen, K., & Weng, B. (2022). Recent progress in Pd-based nanocatalysts for selective hydrogenation. ACS Omega, 7(3), 2456–2472. https://doi.org/10.1021/acsomega.1c06244

[13] Das, A., Mondal, S., Hansda, K. M., Adak, M. K., & Dhak, D. (2023). A critical review on the role of carbon supports of metal catalysts for selective catalytic hydrogenation of chloronitrobenzenes. Applied Catalysis A: General, 651, 118955. https://doi.org/10.1016/j.apcata.2022.118955

[14] Cano, M., Benito, A. M., Urriolabeitia, E. P., Arenal, R., & Maser, W. K. (2013). Reduced graphene oxide: Firm support for catalytically active palladium nanoparticles and game changer in selective hydrogenation reactions. Nanoscale, 5(21), 10189–10193. https://doi.org/10.1039/c3nr02822d

[15] Huang, Y. X., Xie, J. F., Zhang, X., Liong, X., & Yu, H. Q. (2014). Reduced graphene oxide supported palladium nanoparticles via photoassisted citrate reduction for enhanced electrocatalytic activities. ACS Applied Materials & Interfaces, 6(18), 15795–15801. https://doi.org/10.1021/am504664r

[16] Sofian, M., Nasim, F., Ali, H., & Nadeem, M. A. (2023). Pronounced effect of yttrium oxide on the activity of Pd/rGO electrocatalyst for formic acid oxidation reaction. RSC Advances, 13(21), 14306–14316. https://doi.org/10.1039/d3ra01929b

[17] Amer, G. E., Razak, F. I. A., Sapari, S., Nur, H., & Setu, S. A. (2023). Elucidating the alkene hydrogenation reaction based on cotton textile reduced graphene oxide under the influence of external electric field: Illustration of new noble method. Heliyon, 9(4), e14888. https://doi.org/10.1016/j.heliyon.2023.e14888

[18] Yee, S. W., Razak, F. I. A., Sapari, S., Nur, H., Amer, G. E., & Alias, S. S. (2025). Electric field-enhanced hydrogenation catalysis: Modified palladium-graphene oxide composites. Molecular Catalysis, 580, 115132. https://doi.org/10.1016/j.mcat.2025.115132

[19] Shaik, S., Danovich, D., Joy, J., Wang, Z., & Stuyver, T. (2020). Electric-field mediated chemistry: Uncovering and exploiting the potential of (oriented) electric fields to exert chemical catalysis and reaction control. Journal of the American Chemical Society, 142(30), 12551–12568. https://doi.org/10.1021/jacs.0c05128

[20] Kumar, S., Qin, L., & Fan, L. S. (2020). External electric field induced reaction chemistry: A review and perspectives. In ACS Symposium Series (Vol. 1364, pp. 207–227). American Chemical Society. https://doi.org/10.1021/bk-2020-1364.ch008

[21] Lv, J., Sun, R., Yang, Q., Gan, P., Yu, S., & Tan, Z. (2023). Research on electric field—Induced catalysis using single—molecule electrical measurement. Molecules, 28(13), 4968. https://doi.org/10.3390/molecules28134968
[22] Zeng, M., Wu, Y., Liu, Y., Zheng, X., Ying, J., Chen, J., Ren, X., Yang, Z., Feng, R., Zhang, T., Xu, W., Zhang, P., Wang, B., & Cao, X. (2025). Nacre-inspired graphene oxide/chitosan supported Pd species composite paper-like membrane with superior catalytic performance. International Journal of Biological Macromolecules, 306, 141512. https://doi.org/10.1016/j.ijbiomac.2025.141512
[23] Abdulradha, S. K., Hussein, M. T., & Abdulsattar, M. A. (2022). Study of the interaction between reduced graphene oxide and NO_2 gas molecules via density functional theory (DFT). International Journal of Nanoscience, 21(2), 2250009. https://doi.org/10.1142/S0219581X22500090
[24] Jiang, W., Xiang, Z., Xu, B., Li, X., Liu, F., & Fan, G. (2016). Convenient preparation of Pd/RGO catalyst for the efficient hydrodechlorination of various chlorophenols. New Journal of Chemistry, 40, 372-376. https://doi.org/10.1039/c5nj02349a
[25] Elazab, H. A., & El-Idreesy, T. T. (2019). Polyvinylpyrrolidone - Reduced Graphene Oxide - Pd Nanoparticles As An Efficient Nanocomposite For Catalysis Applications In Cross-coupling Reactions. Bulletin of Chemical Reaction Engineering & Catalysis, 14(3), 490-501. https://doi.org/10.9767/bcrc.14.3.3461.490-501
[26] Demirkan, B., Bozkurt, S., Cellat, K., Arikan, K., Yilmaz, M., Savk, A., Calimli, M. H., Nas, M. S., Atalar, M. N., Alma, M. H., & Sen, F. (2020). Palladium supported on polypyrrole/reduced graphene oxide nanoparticles for simultaneous biosensing application of ascorbic acid, dopamine, and uric acid. Scientific Reports, 10, 2946. https://doi.org/10.1038/s41598-020-59935-y
[27] Liu, S., Chen, X., Wu, Z.-J., Zheng, X.-C., Peng, Z.-K., & Liu, P. (2019). Chitosan-reduced graphene oxide hybrids encapsulated Pd(0) nanocatalysts for H_2 generation from ammonia borane. International Journal of Hydrogen Energy, 44, 23610-23619. https://doi.org/10.1016/j.ijhydene.2019.07.088
[28] Frisch, M. J., Trucks, G. W., Schlegel, H. B., Scuseria, G. E., Robb, M. A., Cheeseman, J. R., Scalmani, G., Barone, V., Petersson, G. A., Nakatsuji, H., Li, X., Caricato, M., Marenich, A. V., Bloino, J., Janesko, B. G., Gomperts, R., Mennucci, B., Hratchian, H. P., Ortiz, J. V., Izmaylov, A. F., Sonnenberg, J. L., Williams-Young, D., Ding, F., Lipparini, F., Egidi, F., Goings, J., Peng, B., Petrone, A., Henderson, T., Ranasinghe, D., Zakrzewski, V. G., Gao, J., Rega, N., Zheng, G., Liang, W., Hada, M., Ehara, M., Toyota, K., Fukuda, R., Hasegawa, J., Ishida, M., Nakajima, T., Honda, Y., Kitao, O., Nakai, H., Vreven, T., Throssell, K., Montgomery Jr., J. A., Peralta, J. E., Ogliaro, F., Bearpark, M. J., Heyd, J. J., Brothers, E. N., Kudin, K. N., Staroverov, V. N., Keith, T. A., Kobayashi, R., Normand, J., Raghavachari, K., Rendell, A. P., Burant, J. C., Iyengar, S. S., Tomasi, J., Cossi, M., Millam, J. M., Klene, M., Adamo, C., Cammi, R., Ochterski, J. W., Martin, R. L., Morokuma, K., Farkas, O., Foresman, J. B., & Fox, D. J. (2016). Gaussian 16 Revision C.01. Gaussian Inc.
[29] Al-Otaibi, J. S., Mary, Y. S., Mary, Y. S., Kaya, S., & Erkan, S. (2020). Spectral analysis and DFT investigation of some benzopyran analogues and their self-assemblies with graphene. Journal of Molecular Liquids, 317, 113924. https://doi.org/10.1016/j.molliq.2020.113924
[30] Sameer, A. K., & Hassan, E. K. (2025). Density functional theory calculations for graphene oxide and reduced graphene oxide as a humidity sensor. Sensing and Imaging, 26(1), 6. https://doi.org/10.1007/s11220-025-00684-5